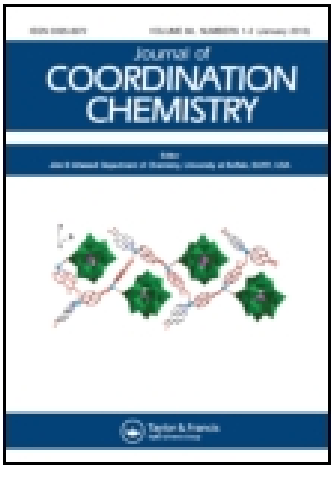

Journal of Coordination Chemistry
Publication details, including instructions for authors and subscription information:
http://www.tandfonline.com/loi/gcoo20

The syntheses, crystal structures, and characterizations of two $Mn^{II/III}$-sandwiching polyoxometalate complexes based on $[\alpha\text{-}SeW_9O_{33}]^{8-}$ units

Yue Zhao[a], Kai-Cheng Xu[a] & Ying Song[a]
[a] Department of Vascular Surgery, The China-Japan Union Hospital of Jilin University, Changchun, China

Accepted author version posted online: 14 Apr 2014.Published online: 08 May 2014.

To cite this article: Yue Zhao, Kai-Cheng Xu & Ying Song (2014) The syntheses, crystal structures, and characterizations of two $Mn^{II/III}$-sandwiching polyoxometalate complexes based on $[\alpha\text{-}SeW_9O_{33}]^{8-}$ units, Journal of Coordination Chemistry, 67:7, 1121-1132, DOI: 10.1080/00958972.2014.914180

To link to this article: http://dx.doi.org/10.1080/00958972.2014.914180

Journal of Coordination Chemistry, 2014
Vol. 67, No. 7, 1121–1132, http://dx.doi.org/10.1080/00958972.2014.914180

The syntheses, crystal structures, and characterizations of two $Mn^{II/III}$-sandwiching polyoxometalate complexes based on $[\alpha\text{-}SeW_9O_{33}]^{8-}$ units

YUE ZHAO, KAI-CHENG XU* and YING SONG

Department of Vascular Surgery, The China–Japan Union Hospital of Jilin University, Changchun, China

(*Received 26 January 2014; accepted 21 March 2014*)

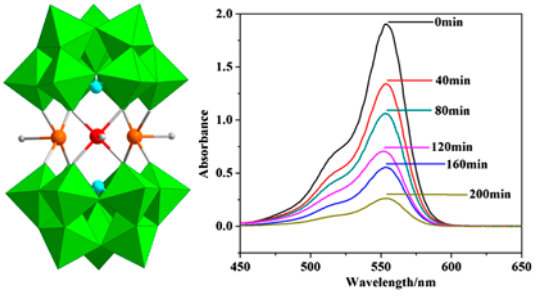

Two new compounds, $K_8[\{Mn^{II}(H_2O)\}_2(WO)(H_2O)(SeW_9O_{33})_2]\cdot 12H_2O$ (**1**) and $K_6[\{Mn^{III}(H_2O)\}_2(WO)(H_2O)(SeW_9O_{33})_2]\cdot 18H_2O$ (**2**), have been synthesized and structurally characterized. Compound **2** represents the first high-valent manganese-substituted POM based on the $[\alpha\text{-}SeW_9O_{33}]^{8-}$ units.

Two sandwich-type polyoxometalates (POM) based on $[\alpha\text{-}SeW_9O_{33}]^{8-}$ building blocks, $K_8[\{Mn^{II}(H_2O)\}_2(WO)(SeW_9O_{33})_2]\cdot 12H_2O$ (**1**) and $K_6[\{Mn^{III}(H_2O)\}_2(WO)(SeW_9O_{33})_2]\cdot 18H_2O$ (**2**), have been synthesized and characterized by elemental analyses, IR, diffuse reflectance UV–vis-NIR spectra, TG, X-ray photoelectron spectroscopy, and single-crystal X-ray diffraction. Electrochemical properties and photocatalytic activities have also been investigated. Single-crystal X-ray diffraction analysis shows that the polyoxoanions of **1** and **2** have similar sandwich structures composed of $[\alpha\text{-}SeW_9O_{33}]^{8-}$ units except for different oxidation states of Mn centers (II for **1**, III for **2**). Compound **2** is the first high-valent trinuclear-manganese (III)-substituted $[\alpha\text{-}SeW_9O_{33}]^{8-}$-based POM. Cyclic voltammograms of **1** and **2** show irreversible redox processes for Mn^{2+} and Mn^{3+}, respectively. Compound **2** has better photocatalytic properties with photocatalytic degradation of Rhodamine-B (RhB) compared to **1**.

Keywords: Polyoxometalate; Sandwich-type; High-valent manganese; Cyclic voltammetry; Photocatalytic property

1. Introduction

The continual interest in transition metal-substituted polyoxometalates (POMs) stems from their potential application in catalysis, molecular adsorption, medicine, electro-conductivity,

*Corresponding author. Emails: xukc2014@gmail.com, Xukc@jlu.edu.cn

magnetism, and photochemistry [1]. Certain properties of such POMs are mainly determined by their transition metal centers, which can be adjusted by using different transition metal ions or changing their nuclearities [2]. High-valent manganese ions ($Mn^{III/IV}$) have received attention attributed to their active redox catalytic activities and their excellent magnetic properties [3]. However, these ions are usually highly instable in aqueous solution compared with other transition metal ions, resulting in difficult synthesis of $Mn^{III/IV}$-substituted POMs. Only a few $Mn^{III/IV}$-substituted polyanions were reported [4], such as $[Mn^{IV}XW_{11}O_{40}H_x]^{n-}$ [4a], $[Mn_2^{III}SiW_{10}O_{40}H_6]^{4-}$ [4b], $[\{Mn^{III}(OH_2)\}_3SiW_9O_{37}]^{7-}$ [4c], $[Mn_3^{II}Mn^{III}(H_2O)_2(PW_9O_{34})_2]^{9-}$, $[Mn^{II}Mn_3^{III}(OH)_2(PW_9O_{34})_2]^{9-}$ [4d], etc. Moreover, their structures are mainly based on the well-known subunits $\{PW_9\}$, $\{SiW_9\}$, $\{AsW_9\}$, etc.

$Mn^{III/IV}$ ions in various lacunary polyanions exhibit different electronic exchange routes and sequentially display different catalytic or magnetic properties [4]. Therefore, to realize a controllable synthesis, it is important to choose suitable lacunary polyanion units to synthesize a series of new $Mn^{III/IV}$-substituted POMs as modifiers to further investigate their catalytic or magnetic properties. Recently, the $[\alpha\text{-}SeW_9O_{33}]^{8-}$ building block has been introduced to an assembly of new POMs. Cronin *et al.* reported a series of polyoxotungstate anions based on $[\alpha\text{-}SeW_9O_{33}]^{8-}$ units [5], such as $\{W_{119}Se_8Fe_2\}$ [5a], $\{Se_2W_{29}O_{103}\}$, $\{Co_{2.5}(W_{3.5}O_{14})(SeW_9O_{33})(Se_2W_{30}O_{107})\}$, $\{CoWO(H_2O)_3(Se_2W_{26}O_{85})(Se_3W_{30}O_{107})_2\}$, $\{Ni_2W_2O_2Cl(H_2O)_3(Se_2W_{29}O_{103})(Se_3W_{30}O_{107})_2\}$, $\{M_2W_nO_m(H_2O)_m(Se_2W_{29}O_{102})_4\}$ (M = Mn, Co, Ni or Zn, $n = 2$, $m = 4$; M = Cu, $n = 3$, $m = 5$), $\{Cu_9Cl_3(H_2O)_{18}(Se_2W_{29}O_{102})_6\}$, $\{(Se_2W_{30}O_{105})_2\}$ [5b], etc. But there are still no high-valent manganese-substituted polyoxoanions consisting of $[\alpha\text{-}SeW_9O_{33}]^{8-}$ reported.

Here, we studied the reactions between $Mn^{III/IV}$ ions and trilacunary polyanion $[\alpha\text{-}SeW_9O_{33}]^{8-}$, and report two new compounds; **2** represents the first high-valent manganese-substituted POM based on $[\alpha\text{-}SeW_9O_{33}]^{8-}$ units.

2. Experimental

2.1. *Materials*

All chemicals were commercially purchased and used without purification.

2.2. *Synthesis of complexes*

2.2.1. $K_8[\{Mn^{II}(H_2O)\}_2(WO)(SeW_9O_{33})_2]\cdot 12H_2O$ (1). A solution of $Na_2WO_4\cdot 2H_2O$ (1.48 g, 4.5 mM) and Na_2SeO_3 (0.087 g, 0.5 mM) in water (10 mL) was acidified with 6 M HCl (5 mL, 45 mM). Then, $MnCl_2\cdot 4H_2O$ (0.15 g, 0.75 mM) in water (10 mL) was added to the above solution. The pH of the resulting cloudy solution was adjusted to 4–5 by the addition of 2 M KOH and heated to 85 °C for 2 h. After being cooled to room temperature, the yellow suspension was filtered and kept at room temperature. Orange crystalline products were isolated after one month (yield 42% based on W). Elemental analysis for $H_{28}K_8Mn_2O_{81}Se_2W_{19}$ (**1**) Calcd Se, 2.93; Mn, 2.04; K, 5.79; W, 64.71 (%); found: Se, 2.99; Mn, 2.00; K, 5.81; W, 64.69. FT/IR data (cm^{-1}): 3420(br), 1623(m), 1546(m), 1393(m), 955(s), 880(s), 775(sh), 692(w).

2.2.2. $K_6[\{Mn^{III}(H_2O)\}_2(WO)(H_2O)(SeW_9O_{33})_2]\cdot 18H_2O$ (2)

The synthesis is similar to **1**, except addition of $K_2S_2O_8$ (0.5 g, 1.9 mM) to the resulting yellow reaction solution of **1** with stirring, and refluxing for 1 h. The color changed from yellow to red brown. After being cooled to room temperature, the suspension was filtered and kept at room temperature. Brown crystals of **2** were isolated after two weeks (yield 45% based on W). Elemental analysis for $H_{40}K_6Mn_2O_{87}Se_2W_{19}$ (**2**) Calcd Se, 2.91; Mn, 2.02; K, 4.32; W, 64.36 (%); found: Se, 2.90; Mn, 2.00; K, 4.36; W, 64.39 (%). FT/IR data (cm^{-1}): 3425(br), 1624(m), 1536(m), 1393(m), 953(s), 881(s), 778(sh), 690(w).

2.3. *Physical measurements*

Elemental analyses for W, Se, Mn, and K were performed in a Leaman inductively coupled plasma spectrometer. IR spectra were recorded from 400 to 4000 cm^{-1} on an Alpha Centaurt FT/IR Spectrophotometer with pressed KBr pellets. Diffuse reflectance UV–vis spectra ($BaSO_4$ pellet) were obtained with a Varian Cary 500 UV–vis NIR spectrometer. TG analyses were carried out on a Perkin-Elmer TGA7 instrument in flowing N_2 with a heating rate of 10 °C min^{-1}. X-ray photoelectron spectroscopy (XPS) analyses were performed on a VG ESCALABMKII spectrometer with a Mg-$K\alpha$ (1253.6 eV) achromatic X-ray source. The vacuum inside the analysis chamber was maintained at 6.2×10^{-6} Pa during the analysis.

2.4. *Electrochemical experiment*

Electrochemical measurements and data collections were carried out on a CHI 660 electrochemical workstation connected to a personal computer at room temperature (25–30 °C). The pH was tested by a pHS-25B-type pH meter. A conventional three-electrode system was used. The working electrode was a glassy carbon. Platinum wire was used as the counter electrode and Ag/AgCl was used as the reference electrode. Thrice distilled water was used throughout the experiments. All the experiments were conducted at room temperature (25–30 °C). Cyclic voltammograms were recorded on 1 mM solutions in 0.5 M H_2SO_4/Na_2SO_4 at pH 4.5 for **1** and **2**.

2.5. *Photocatalysis experiments*

Aqueous solutions were prepared from the addition of the sample (30 mg for **1** or **2**) to a 50 mL 0.5 M H_2SO_4/Na_2SO_4 (pH 4.50) solution of RhB dye (2×10^{-5} M) with magnetically stirring it in the dark for 50 min, then the solution was exposed to UV irradiation from a 125 W Hg lamp which was at a distance of 3–4 cm between the liquid surface and the lamp, with continuous stirring. At different time intervals, 3 mL of samples was taken and was used for UV–vis absorption spectrum analysis.

2.6. *Single-crystal X-ray diffraction*

The crystallographic data of **1** and **2** were collected at 293(2) K on a Rigaku R-axis Rapid IP diffractometer using graphite monochromated-Mo-$K\alpha$ radiation ($\lambda = 0.71073$ Å). Data processing was accomplished with the RAXWISH processing program. A total of 42,657 reflections for **1** were collected, of which 14,868 reflections were unique, a total of 21,862

Table 1. Crystal data and structure refinements for **1** and **2**.

Complex	**1**	**2**
Chemical formula	$H_{28}K_8Mn_2O_{81}Se_2W_{19}$	$H_{40}K_6Mn_2O_{87}Se_2W_{19}$
Formula weight (M)	5397.97	5427.68
Temperature (K)	293(2)	293(2)
Wavelength (Å)	0.71073	0.71073
Crystal system	Monoclinic	Hexagonal
Space group	*P*2(1)/*n*	*P*63/*mmc*
a (Å)	17.3877(19)	16.563(2)
b (Å)	22.526(2)	16.563(2)
c (Å)	22.949(2)	18.738(2)
α (°)	90	90
β (°)	109.718(2)	90
γ (°)	90	120
V (Å^3)	8461.6(16)	4451.8(9)
Z	4	2
D_{Calcd} (g/cm^3)	4.237	4.049
μ (Mo Kα) (mm^{-1})	27.357	25.914
F (0 0 0)	9408	4746
Goodness-of-fit on F^2	0.995	1.092
R_1[a]	0.0721	0.0338
wR_2[b]	0.1709	0.0943

[a] $R_1 = \Sigma||F_0| - |F_c||/\Sigma|F_0|$.
[b] $wR_2 = \Sigma[w(F_0^2 - F_c^2)^2]/\Sigma[w(F_0^2)^2]^{1/2}$.

reflections for **2** were collected, of which **1508** reflections were unique. The structures of **1** and **2** were solved by direct methods and refined by full-matrix least-squares on F^2 using the SHELXTL-97 crystallographic software package [6]. Crystal data and structure refinements for **1** and **2** are summarized in table 1. During the refinement of **1**, the W20, Mn2, and Mn3 sites are size-occupancy disordered with the occupancies of 30% (70%) for W19 (Mn1), 40% (60%) for W20 (Mn2), and 30% (70%) for W21 (Mn3), respectively. During the refinement of **2**, the W2, Mn1A, Mn1B sites are size-occupancy disordered with the occupancies of 33% (67%) for W2 (Mn1), 33% (67%) for W2A (Mn1A), and 33% (67%) for W2B (Mn1B), separately.

3. Results and discussion

3.1. *Synthesis discussion*

The isolations of **1** and **2** depend on one-pot synthesis. This synthetic process also involves formation of lacunary polyoxoanion building blocks. The {α-SeW_9O_{33}} units were obtained from adjustment of the pH value of the mixture of $Na_2WO_4{\cdot}2H_2O$, Na_2SeO_3 and 6 M HCl in aqueous solution.

Three factors should be emphasized in the synthesis of **1** and **2**. First, the final pH of the reaction system should be kept in the pH range 4.0–5.0. It can be speculated that the trivacant Keggin-type species [α-SeW_9O_{33}]$^{8-}$ might be stable in this pH range, because no crystalline phase can be obtained out of this pH range. Second, the use of Na_2SeO_3 seems to be as a reactant and also a suitable synthetic template for assembly of the polyoxoanions. Third, the amount of potassium persulphate is another key factor in synthesis of **2**. The color of the solution changed from yellow to red brown, which indicated that Mn^{2+} cations were oxidized to Mn^{3+}.

3.2. *Structure description*

The single-crystal X-ray diffraction analysis shows that the polyanion of **1** is constructed from two $[\alpha\text{-}SeW_9O_{33}]^{8-}$ moieties, one {WO} fragment and two $\{Mn^{II}(H_2O)\}$ units by W–O–M (M=W or Mn) connection, leading to a sandwich-type structure (see figure 1). All $[\alpha\text{-}SeW_9O_{33}]^{8-}$ units possess the well-known trivacant Keggin structural B-α-type, resulting from removal of three edge-sharing $\{WO_6\}$ octahedra in α-Keggin-type structure. Bond Valence Sum (BVS) calculations indicate that all Se, W, and Mn sites possess +4, +6, and +2 oxidation states, respectively (see table S3, see online supplemental material at http://dx.doi.org/10.1080/00958972.2014.914180) [7]. All W and Mn sites in the sandwich part exhibit square–pyramid five coordination, the W–O bond lengths are 1.63(3)–2.50(2) Å and O–W–O bond angles vary from 90.0(15)° to 173.6(14)°. Mn^{II}–O bond lengths are 1.98(3)–2.49(4) Å and the O–Mn^{II}–O angles vary from 86.7(10)° to 175.2(10)° (see table S1). All three metal centers in the sandwiching part are disordered, the {WO} unit and two $\{Mn^{II}(H_2O)\}$ units share the three parts with the occupancies of 30% (70%) for W19 (Mn1), 40% (60%) for W20 (Mn2), and 30% (70%) for W21 (Mn3), respectively [see figure 1(b)]. Three potassium cations are also coordinated to the central sandwich, alternately residing in the three transition metal centers [see figure 1(b)]. The polyanion was charge-balanced by another five potassium cations. Twelve crystalline waters were coordinated to the counter-cations or isolated into the crystal structure.

The structure of the polyanion in **2** is similar to **1**, but there are no potassium cations coordinated to the three metal centers via oxygen (see figure 3). All three metal centers are disordered, that is, the {WO} and two $\{Mn^{III}(H_2O)\}$ units share the three parts with the occupancies of 33% (67%) for W2 (Mn1), 33% (67%) for W2A (Mn1A), and 33% (67%) for W2B (Mn1B) (see figure 3). The W–O bond lengths are 1.709(12)–2.417(11) Å and O–W–O bond angles vary from 100.9(5)° to 172.4(5)° (see table S2). The Mn^{III}–O bond lengths are 1.887(8)–2.31(2) Å. The polyanion in **2** is charge-balanced by six potassium cations. The BVS calculations show that the oxidation states of Se, W, and Mn sites were

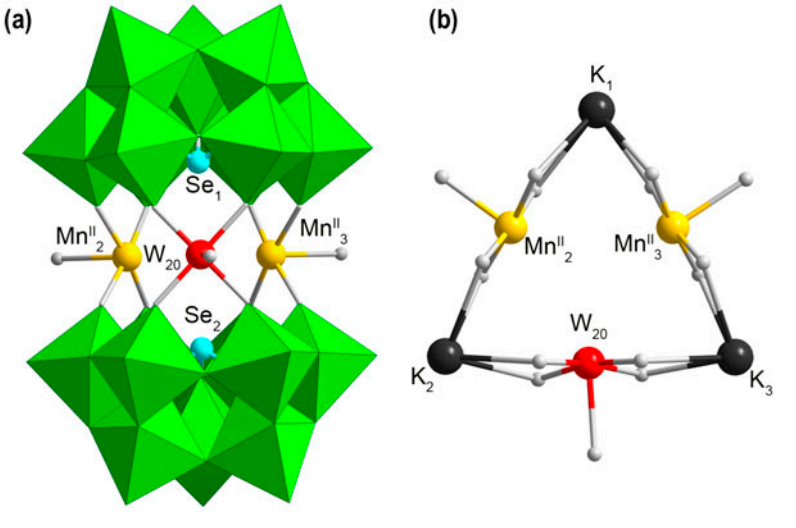

Figure 1. (a) Polyhedral and ball–stick representation of **1**; (b) Ball-and-stick view of the sandwich part of **1**. The color code is as follows: W (red), Mn (yellow), Se (cyan), O (light gray), and K (dark gray), see http://dx.doi.org/10.1080/00958972.2014.914180 for color version.

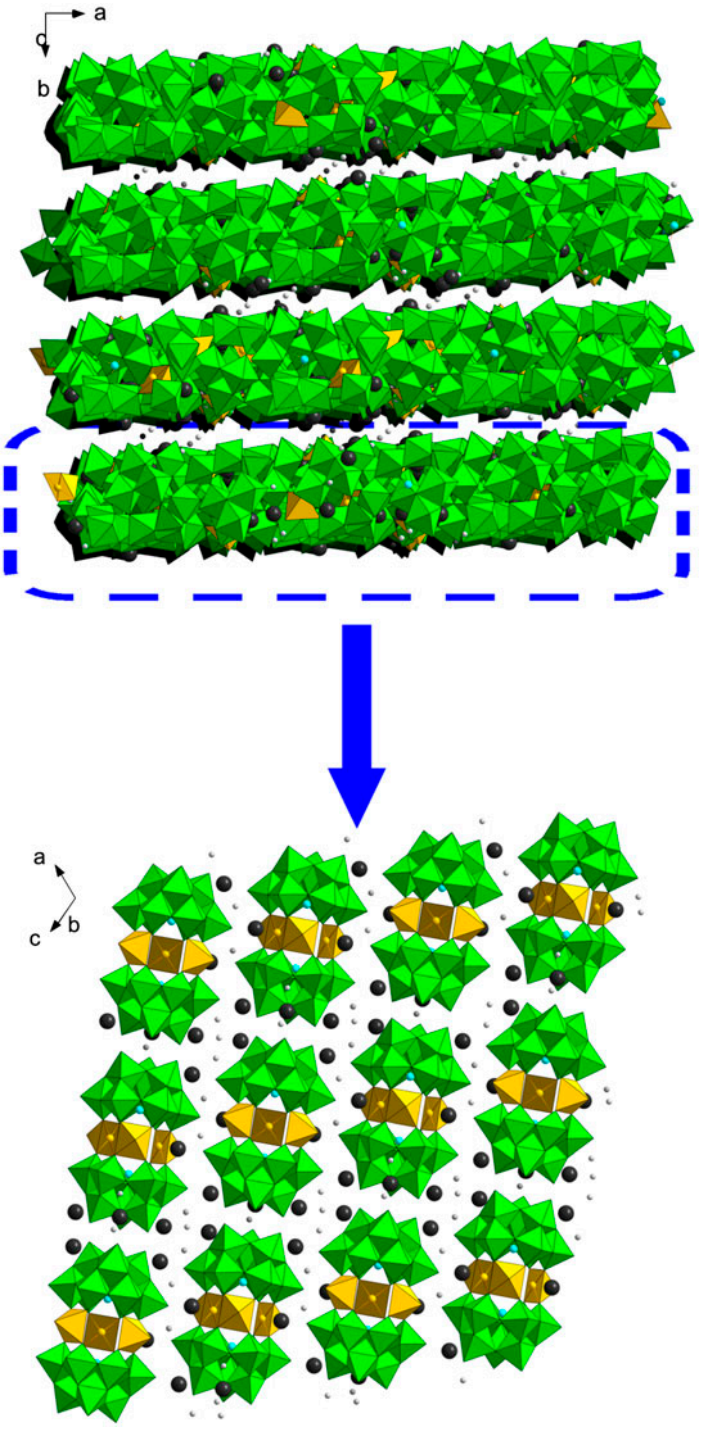

Figure 2. 3-D packing arrangement of **1**. All hydrogens and K–O bonds are omitted for clarity. Color codes: $\{MnO_5\}$, yellow polyhedron; $\{WO_6\}$, green octahedron, O (light gray), and K (dark gray) are shown with thick sticks (see http://dx.doi.org/10.1080/00958972.2014.914180 for color version).

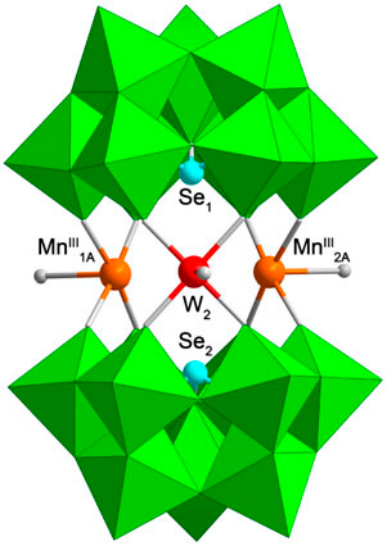

Figure 3. Polyhedral and ball–stick representation of **2**. The color code is as follows: W (red), Mn (yellow), Se (cyan), O (light gray), and K (dark gray), see http://dx.doi.org/10.1080/00958972.2014.914180 for color version.

+4, +6, and +3, respectively (see table S4) [7]. In the packing arrangement, adjacent sandwiching polyanions of **1** and **2** are connected by K^+ to form a three-dimensional (3-D) open framework (see figures 2 and 4).

Sandwich-type POTs (such as compounds **1** and **2**), contain a certain number of transition metal cations sandwiched by two lacunary species, which are based on trivacant Keggin $\{XW_9\}$ (X = Si, Ge, P, As, Sb, Bi, etc.) representing the largest subfamily of POMs [8]. Especially the $\{W_9O_{33}\}$ groups templating by the heteroanions SeO_3^{2-} or SbO_3^{3-} achieve the $\{\alpha\text{-}SeW_9O_{33}\}$ or $\{B\text{-}\alpha\text{-}SbW_9O_{33}\}$ units [9], respectively. These two species possess two main features: (1) two heteroanions with a lone pair of electrons that easily allows "open" Keggin units to form; (2) two $\{\alpha\text{-}SeW_9O_{33}\}$ units link three metal cations, whereas, two $\{B\text{-}\alpha\text{-}SbW_9O_{33}\}$ units may link four metal cations. Different metal cations in the center result in different sandwich motifs.

3.3. *FT-IR spectroscopy*

IR spectra of **1** and **2** are similar. The IR spectrum of **1** (see figure S1) shows a broad peak at 3420 cm^{-1} and strong peak at 1623 cm^{-1} attributed to the lattice and coordinated water. The characteristic peaks at 955, 880, 775, and 692 cm^{-1} correspond to ν(Se–O), ν(W=O_d), ν(W–O_b), and ν(W–O_c), respectively. In the IR spectrum of **2** (see figure S2), a broad peak at 3425 cm^{-1} and strong peak at 1624 cm^{-1} are ascribed to lattice and coordinated water. The characteristic peaks at 953, 881, 778, and 690 cm^{-1} can be identified to ν(Se–O), ν(W=O_d), ν(W–O_b), and ν(W–O_c) vibrations, respectively.

3.4. *TG analyses*

The TG curve of **1** shows two continual weight losses (see figure S3). The first from 50 to 100 °C corresponds to loss of all coordinated water in **1**. The value of ca. 0.67% is in accord

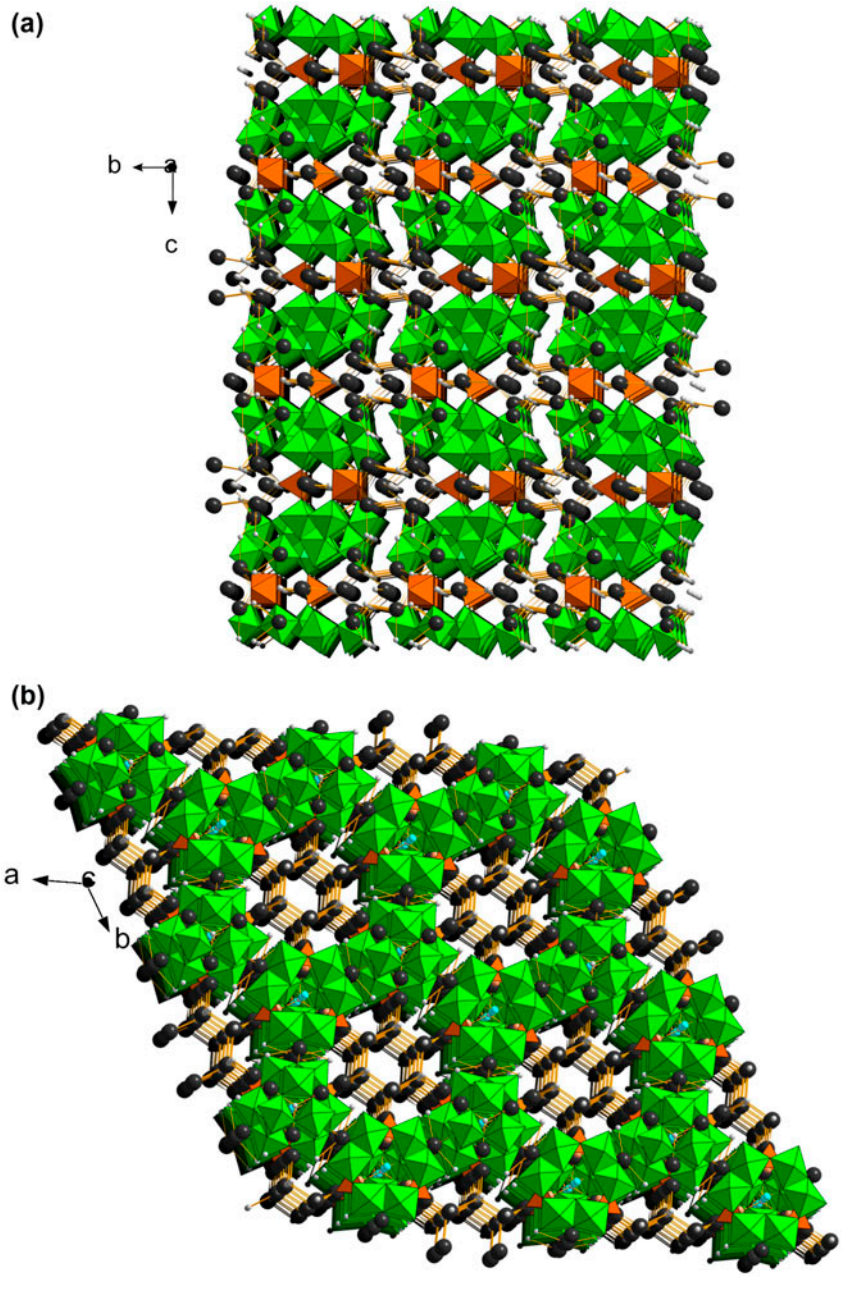

Figure 4. 3-D packing arrangement of **2**. Color codes: {MnO_5}, orange polyhedron; {WO_6}, green octahedron, O (light gray), and K (dark gray) are shown with thick sticks, see http://dx.doi.org/10.1080/00958972.2014.914180 for color version.

with the calculated value of 0.66% (~$2H_2O$). The second weight loss of ca. 4.00% (the calculated value is 3.99%) from 100 to 200 °C might be lattice waters, and then the structure began to decompose. TG curve of **2** (see figure S4) shows a weight loss of ca. 0.66% from 40 to

70 °C, ascribed to loss of all coordinated water, consistent with the calculated value of 0.67% (~$2H_2O$). Another weight loss of ca. 6.00% (the calculated value is 5.97%) from 70 to 200 °C might be lattice waters, and then the structure began to decompose.

3.5. *XPS analyses*

XPS was performed to identify the oxidation states of Mn in **1** and **2**. XPS spectrum of **1** [see figure S5(a)] exhibits one peak at 640.4 eV in the energy region of Mn $2p_{3/2}$ and another peak at 651.7 eV in the energy region of Mn $2p_{1/2}$. The distance between two main peaks is about 11.3 eV, which is consistent with the Mn^{II} centers [10a]. The XPS for **2** [see figure S5(b)] shows two peaks at ca. 641.2 and ca. 652.7 eV in the energy region of Mn $2p_{3/2}$ and Mn $2p_{1/2}$, respectively, with a distance between two main peaks of 11.5 eV, confirming that all the Mn centers in **2** possess +3 oxidation state [10]. These results are in agreement with the BVS calculations.

3.6. *Electrochemical behavior*

The cyclic voltammogram (CV) of **1** [see figure 5(a)] shows a reversible peak at $E_{1/2} = (E_{pa} + E_{pc})/2 = +749$ mV (IV/IV′), corresponding to the Mn^{II} redox processes, and two quasi-reversible peaks at $E_{1/2} = -852$ (I/I′) and –512 mV (II/II′), one irreversible anodic peak at –16 mV (III/III′) ascribed to W^{VI} redox processes. Compared with **1**, the CV of **2** [see figure 5(c)] also shows two similar quasi-reversible peaks at $E_{1/2} = -835$ (I/I′) and –495 mV

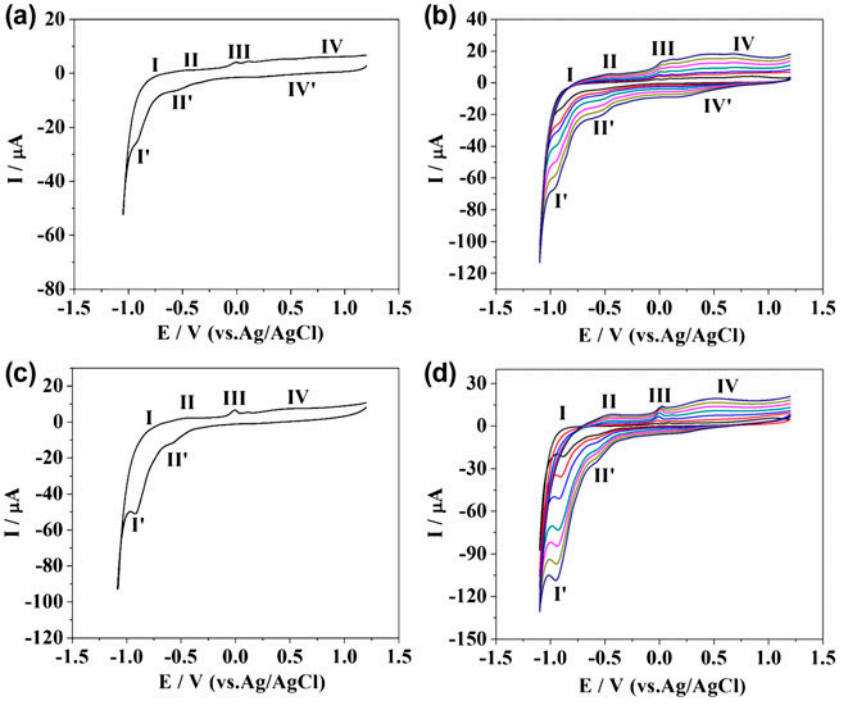

Figure 5. Cyclic voltammograms of **1** and **2** in 0.5 M H_2SO_4/Na_2SO_4 buffer solution. The scan rate was 50 mVs^{-1}: (a) **1**, (c) **2**. Cyclic voltammograms at different scan rates: (b) **1**, (d) **2**. From inside to out: 20, 50, 80, 100, 200, 300, 400, and 500 mVs^{-1}. The working electrode was glassy carbon and the reference electrode was Ag/AgCl.

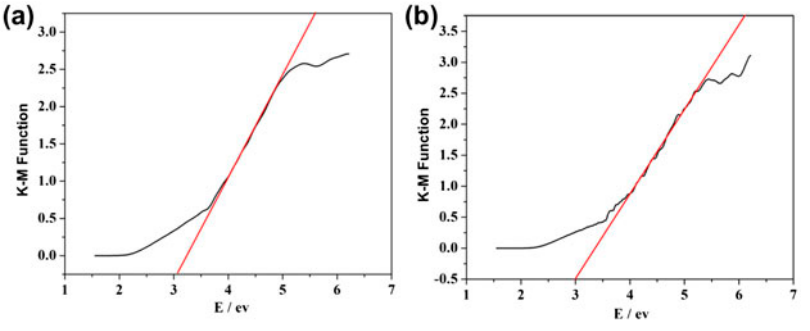

Figure 6. Diffuse reflectance UV–vis spectra of **1** (a) and **2** (b).

(II/II′), and one irreversible anodic peak at –12 mV (III/III′) attributed to W^{VI} redox processes. One blurry and irreversible anodic peak at +515 mV (IV/IV′), indicating Mn^{III} redox processes, probably results from the slow electron transfer rather than chemical irreversibility. This may be explained by the Jahn–Teller effect existing in high-valent manganese-substituted POMs, especially for Mn^{III} [11]. The CVs for **1** and **2** at different scan rates suggest that they are stable in solution [see figure 5(b) and (d)].

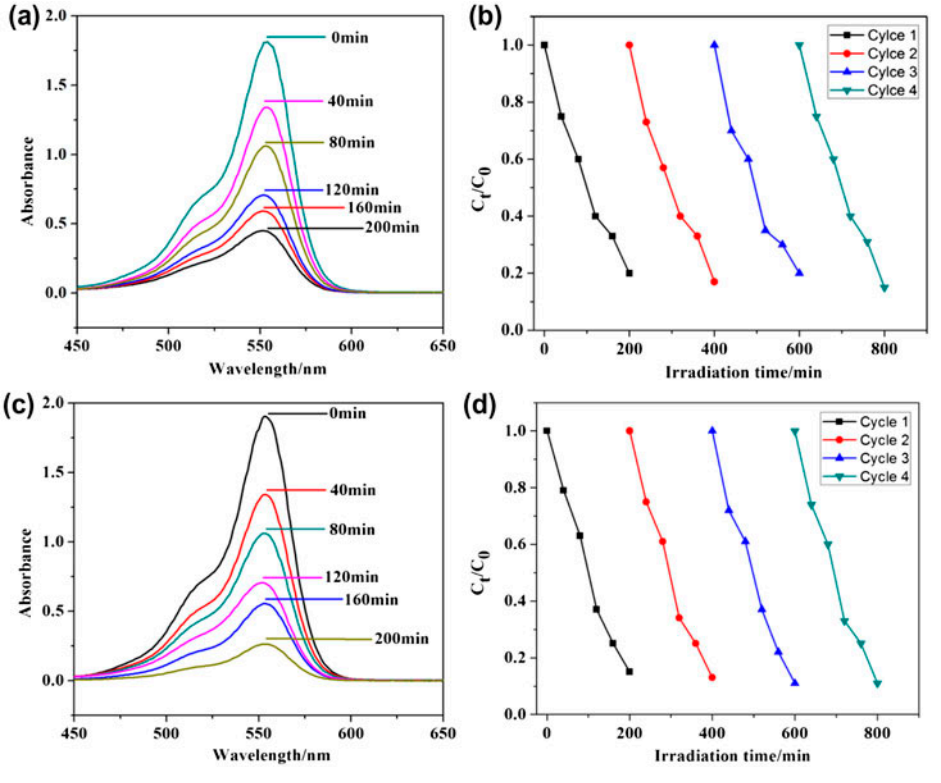

Figure 7. The UV–vis absorption spectra of **1** (a) and **2** (c) recorded at a 0.5 M H_2SO_4/Na_2SO_4 solution at pH 4.50 including 2×10^{-5} M RhB. Four cycles of RhB degradation tests by **1** (b) and **2** (d). At the irradiation time of 200, 400, 600, and 800 min, RhB (3 mL) was added to the reaction system.

3.7. *Photocatalytic activities*

In order to test the conductivity of **1** and **2**, the diffuse reflectance UV–vis-NIR spectra of the powder crystal samples were measured to obtain their band gap (E_g) (see figure 6). For **1** and **2**, the band gaps of E_g were 3.09 and 3.00 eV, respectively, which represents two new types of semiconductor materials. On the basis of the band gaps, the photocatalytic degradations of Rhodamine-B (RhB) were investigated in the presence of **1** and **2** as the photocatalysts (see figure 7) [12]. During irradiation, the changes in the UV–vis absorption spectra of aqueous RhB solutions with **1** and **2** as the photocatalysts indicate that the UV–vis absorbance ($\lambda = 554$ nm) of RhB decreases upon irradiation times from 0 to 200 min, which may indicate the photocatalytic activities of **1** and **2** [see figure 7(a) and (c)]. The conversions of RhB with **1** and **2** as the photocatalysts calculated from the concentrations of RhB *versus* reaction time plotted in figure 7 are 84% for **1** and 77% for **2**, respectively. Four cycles of RhB degradation tests show that the values of C_t/C_0 decrease with increasing reaction time (C_t is the RhB concentration at the time of t; C_0 is the RhB concentration at the start of radiation) [13], which prove the stability of the catalytic degradation processes [see figure 7(b) and (d)].

4. Conclusion

We have synthesized and characterized two new $Mn^{II/III}$-substituted polyanions based on $[\alpha\text{-}SeW_9O_{33}]^{8-}$. Compound **2** represents the first high-valent manganese-substituted POM based on $[\alpha\text{-}SeW_9O_{33}]^{8-}$ units. The CV of **2** shows an irreversible Mn^{III} redox process, probably owing to a slow electron transfer step. Photocatalytic degradations of RhB indicate that **2** has better photocatalytic activity than **1**. In the field of $\{XW_9O_{33}\}$-based high-nuclearity clusters, polyoxoanions containing some other heterogroups with the lone pair of electrons as Se^{IV} (e.g. As^{III}, Sb^{III}) may also give new architectures along with different metal centers. Synthesis of **2** confirms the possibilities of preparing new $Mn^{III/IV}$-substituted POMs with various lacunary polyanions and work in this field is underway.

Supplementary material

The selected bond lengths and bond angles, bond valence sum calculations, IR spectra, TG curves, and XPS spectra of **1** and **2** are in the supporting information. Crystallographic data for the structural analysis have been deposited with the Cambridge Crystallographic Data Center, CCDC reference numbers: 982174 for **1** and 982175 for **2**. These data can be obtained free of charge at www.ccdc.cam.ac.uk/conts/retrieving.html (or from the Cambridge Crystallographic Data Center, 12 Union Road, Cambridge CB2 1EZ, UK; Fax: +44 1223/336 033; Email: deposit@ccdc.cam.ac.uk).

Funding

This work was supported by the Technology Services Foundation of Jilin University [grant number 3R211W233430].

References

[1] (a) G.N. Newton, G.J.T. Cooper, P. Kögerler, D.L. Long, L. Cronin. *J. Am. Chem. Soc.*, **130**, 790 (2008); (b) S.T. Zheng, J. Zhang, X.X. Li, W.H. Fang, G.Y. Yang. *J. Am. Chem. Soc.*, **132**, 15102 (2010); (c) J.J. Stracke, R.G. Finke. *ACS Catal.*, **4**, 79 (2014); (d) Z.M. Zhang, Y.G. Li, E.B. Wang, X.L. Wang, C. Qin, H.Y. An. *Inorg. Chem.*, **45**, 4313 (2006); (e) J.W. Zhao, D.Y. Shi, L.J. Chen, P.T. Ma, J.P. Wang, J. Zhang, J.Y. Niu. *Cryst. Growth Des.*, **13**, 4368 (2013); (f) P.C. Yin, T. Li, R.S. Forgan, C. Lydon, X.B. Zuo, Z.N. Zheng, B. Lee, D.L. Long, L. Cronin, T.B. Liu. *J. Am. Chem. Soc.*, **135**, 13425 (2013); (g) Y. Yang, B. Zhang, Y.Z. Wang, L. Yue, W. Li, L.X. Wu. *J. Am. Chem. Soc.*, **135**, 14500 (2013).

[2] (a) J.M. Clemente-Juan, E. Coronado. *Coord. Chem. Rev.*, **361**, 193 (1999); (b) Q. Wu, Y.G. Li, Y.H. Wang, E.B. Wang, Z.M. Zhang, R. Clérac. *Inorg. Chem.*, **48**, 1606 (2009); (c) H.M. Zhang, Y.G. Li, Y. Lu, R. Clérac, Z.M. Zhang, Q. Wu, X.J. Feng, E.B. Wang. *Inorg. Chem.*, **48**, 10889 (2009); (d) U. Kortz, N.K. Al-Kassem, M.G. Savelieff, N.A. Al Kadi, M. Sadakane, *Inorg. Chem.*, **40**, 4742 (2001); (e) B.S. Bassil, S. Nellutla, U. Kortz, A.C. Stowe, J. van Tol, N.S. Dalal, B. Keita, L. Nadjo. *Inorg. Chem.*, **44**, 2659 (2005); (f) L.H. Bi, U. Kortz, S. Nellutla, A.C. Stowe, J. van Tol, N.S. Dalal, B. Keita, L. Nadjo. *Inorg. Chem.*, **44**, 896 (2005); (g) B.S. Bassil, M.H. Dickman, U. Kortz. *Inorg. Chem.*, **45**, 2394 (2006).

[3] (a) X.Y. Zhang, M.T. Pope. *J. Mol. Catal. A: Chem.*, **114**, 201 (1996); R. Sessoli, H.L. Tsai, A.R. Schake, S. Wang, J.B. Vincent, K. Folting, D. Gatteschi, G. Christou, D.N. Hendrickson. *J. Am. Chem. Soc.*, **115**, 1804 (1993); (c) G. Christou, D. Gatteschi, D.N. Hendrickson, R. Sessoli. *MRS Bull.*, **25**, 66 (2000).

[4] (a) X.Y. Zhang, M.T. Pope, M.R. Chance, G.B. Jameson. *Polyhedron*, **14**, 1381 (1995); (b) X.Y. Zhang, C.J. O'Connor, G.B. Jameson, M.T. Pope. *Inorg. Chem.*, **35**, 30 (1996); (c) J.F. Liu, F. Ortega, M.T. Pope. *J. Chem. Soc., Dalton Trans.*, 1901 (1992); (d) X.Y. Zhang, C.J. O'Connor, G.B. Jameson, M.T. Pope. *Polyhedron*, **15**, 917 (1996); (e) P. Mialane, C. Duboc, J. Marrot, E. Riviere, A. Dolbecq, F. Secheresse. *Chem. Eur. J.*, **12**, 1950 (2006).

[5] (a) J. Yan, J. Gao, D.L. Long, H.N. Miras, L. Cronin. *J. Am. Chem. Soc.*, **132**, 11410 (2010); (b) J. Gao, J. Yan, S. Beeg, D.L. Long, L. Cronin. *J. Am. Chem. Soc.*, **135**, 1796 (2013).

[6] (a) G.M. Sheldrick. *SHELXL-97, Program for Crystal Structure Refinement*, University of Göttingen, Germany (1997); (b) G.M. Sheldrick. *SHELXS-97, Program for Crystal Structure Solution*, University of Göttingen, Germany (1997).

[7] I.D. Brown, D. Altermatt. *Acta Crystallogr.*, **B41**, 244 (1985).

[8] (a) O. Oms, A. Dolbecq, P. Mialane. *Chem. Soc. Rev.*, **41**, 7497 (2012); (b) S.T. Zheng, G.Y. Yang. *Chem. Soc. Rev.*, **41**, 7623 (2012).

[9] (a) Z.S. Wang, Z.M. Zhang, Y.G. Li, X.B. Han, H. Duan, E.B. Wang. *J. Coord. Chem.*, **65**, 1443 (2012); (b) Q. Shan, K. Yu, C.X. Wang, Z.H. Su, J. Gu, B.B. Zhou. *J. Coord. Chem.*, **66**, 402 (2013);

[10] (a) Y.F. Han, F. Chen, Z. Zhong, K. Ramesh, L. Chen, E. Widjaja. *J. Phys. Chem. B*, **110**, 24450 (2006); (b) Q. Wu, Y.G. Li, Y.H. Wang, E.B. Wang, Z.M. Zhang, R. Clérac. *Inorg. Chem.*, **48**, 1606 (2009); (c) F. Moro, V. Corradini, M. Evangelisti, V. De Renzi, R. Biagi, U. del Pennino, C.J. Milios, L.F. Jones, E.K. Brechin. *J. Phys. Chem. B*, **112**, 9729 (2008).

[11] (a) B.S. Bassil, S. Nellutla, U. Kortz, A.C. Stowe, J. van Tol, N.S. Dalal, B. Keita, L. Nadjo. *Inorg. Chem.*, **44**, 2659 (2005); (b) L.H. Bi, U. Kortz, S. Nellutla, A.C. Stowe, J. van Tol, N.S. Dalal, B. Keita, L. Nadjo. *Inorg. Chem.*, **44**, 896 (2005); (c) L.H. Bi, U. Kortz. *Inorg. Chem.*, **43**, 7961 (2004); (d) H.Y. An, E.B. Wang, D.R. Xiao, Y.G. Li, Z.M. Su, L. Xu. *Angew. Chem. Int. Ed.*, **45**, 904 (2006).

[12] (a) K. Lv, Y.M. Xu. *J. Phys. Chem. B*, **110**, 6204 (2006); (b) C.C. Chen, W. Zhao, P.X. Lei, J.C. Zhao, N. Serpone. *Chem. Eur. J.*, **10**, 1956 (2004).

[13] (a) J.M. Gu, S.H. Li, E.B. Wang, Q.Y. Li, G.Y. Sun, R. Xu, H. Zhang. *J. Solid State Chem.*, **182**, 1265 (2009); (b) L.L. Li, Y. Chu, Y. Liu, L.H. Dong. *J. Phys. Chem. C*, **111**, 2123 (2007).